unknown fields, the condition numbers of the resulting matrices are kept relatively small even when the permittivity is large. Compared with the exact solutions, it is seen that the accuracy is reasonably good.

It is seen that the norm $\|A^{-1}\|$ of the present method increases somewhat with the permittivity. The condition number of the matrix will be improved further if this norm can be reduced.

References

[1] J. H. Richmond, "Scattering by a dielectric cylinder of arbitrary cross section shape," *IEEE Trans. Antennas Propagat.*, vol. AP-13, pp. 334–341, May 1965.

[2] J. H. Richmond, "TE-wave scattering by a dielectric cylinder of arbitrary cross-section shape," *IEEE Trans. Antennas Propagat.*, vol. AP-14, pp. 460–464, July 1966.

[3] D. E. Liversay and K. M. Chen, "Electromagnetic fields induced inside arbitrarily shaped biological bodies," *IEEE Trans. Microwave Theory Tech.*, vol. MTT-22, pp. 1273–1280, Dec. 1974.

[4] D. T. Borup and O. P. Gandhi, "Calculation of high-resolution SAR distribution in biological bodies using the FFT algorithm and conjugate gradient method," *IEEE Trans. Microwave Theory Tech.*, vol. MTT-33, pp. 417–419, May 1985.

[5] C. C. Su, "Calculation of electromagnetic scattering from a dielectric cylinder using the conjugate gradient method and FFT," *IEEE Trans. Antennas Propagat.*, vol. AP-35, pp. 1418–1425, Dec. 1987. (The $\bar{\epsilon}$ and $W(\phi)\lambda$ in (7) and (23b) therein are misprints of $\bar{E}$ and $W(\phi)/\lambda$, respectively.)

[6] C. C. Su, "Electromagnetic scattering by a dielectric body with arbitrary inhomogeneity and anisotropy," *IEEE Trans. Antennas Propagat.*, vol. 37, pp. 384–389, Mar. 1989.

[7] A. F. Peterson and R. Mittra, "Convergence of the conjugate gradient method when applied to matrix equations representing electromagnetic scattering problems," *IEEE Trans. Antennas Propagat.*, vol. AP-34, pp. 1447–1454, Dec. 1986.

[8] D. T. Borup, D. M. Sullivan, and O. P. Gandhi, "Comparison of the FFT conjugate gradient method and the finite-difference time-domain method for the 2-D absorption problem," *IEEE Trans. Microwave Theory Tech.*, vol. MTT-35, pp. 383–395, Apr. 1987.

[9] H. Massoudi, C. H. Durney, and M. F. Iskander, "Limitations of the cubical block model of man in calculating SAR distribution," *IEEE Trans. Microwave Theory Tech.*, vol. MTT-32, pp. 746–752, Aug. 1984.

[10] M. J. Hagmann, H. Massoudi, C. H. Durney, and M. F. Iskander, "Comments on 'Limitations of the cubical block model of man in calculating SAR distribution'," *IEEE Trans. Microwave Theory Tech.*, vol. MTT-33, pp. 347–350, Apr. 1985.

[11] S. C. Hill, C. H. Durney, and D. A. Christensen, "Numerical calculations of low-frequency TE fields in arbitrarily shaped inhomogeneous lossy dielectric cylinders," *Radio Sci.*, vol. 18, pp. 328–336, May 1983.

[12] D. H. Schaubert, D. R. Wilton, and A. W. Glisson, "A tetrahedral modeling method for electromagnetic scattering by arbitrarily shaped, inhomogeneous dielectric bodies," *IEEE Trans. Antennas Propagat.*, vol. AP-32, pp. 77–85, Jan. 1984.

[13] C. T. Tsai, H. Massoudi, C. H. Durney, and M. F. Iskander, "A procedure for calculating fields inside arbitrarily shaped inhomogeneous dielectric bodies using linear basis functions with the moment method," *IEEE Trans. Microwave Theory Tech.*, vol. MTT-34, pp. 1131–1138, Nov. 1986. (For comments, see vol. MTT-35, pp. 785–786, Aug. 1987.)

[14] C. C. Su, "Fast algorithm for transversely inhomogeneous optical fibres using power method and fast Fourier transform," *Proc. Inst. Elec. Eng.*, vol. 134, pt. J, pp. 276–280, Oct. 1987.

[15] C. C. Su, "A surface integral equations method for homogeneous optical fibers and coupled image lines of arbitrary cross sections," *IEEE Trans. Microwave Theory Tech.*, vol. MTT-33, pp. 1114–1119, Nov. 1985.

[16] A. V. Oppenheim and R. W. Schafer, *Digital Signal Processing*. Englewood Cliffs, NJ: Prentice-Hall, 1976, p. 110.

[17] A Ralston and P. Rabinowitz, *A First Course in Numerical Analysis*, 2nd ed. New York: McGraw-Hill, 1978.

[18] R. Harrington, *Time-Harmonic Electromagnetic Fields*. New York: McGraw-Hill, 1961, p. 261.

A Dipole Antenna for Interstitial Microwave Hyperthermia

W. Hürter, F. Reinbold, and W. J. Lorenz

Abstract—**An improved interstitial microwave antenna design was investigated in static phantom experiments at 915 MHz and different insertion depths. Compared with conventional interstitial antennas, the dipole microwave antenna presented in this paper shows heating patterns which are concentrated on the dipole irrespective of the insertion depth. By analogy to interstitial radiotherapy, the microwave antenna we have developed thus allows a high concentration of energy in the target volume with as little damage as possible to the healthy surrounding tissue. The undesired heating of healthy tissue along the feeding line observed with conventional interstitial antennas is avoided. A $\lambda/4$ sleeve on the feeding line (which does not radiate microwave energy itself to the surrounding tissue) transforms an open end, i.e., a high impedance at the generator end of the dipole antenna. The current flowing back along the outside of the outer conductor of the feeding line in the direction of the generator is 0 at this point. Both dipole sections thus have the same terminating impedance. Since the $\lambda/4$ sleeve is mounted outside the antenna, its mechanical length is not restricted by the mechanical length of the antenna. It can hence be charged with dielectric materials of low dielectricity constants, e.g. PTFE.**

I. Introduction

Results from basic research and clinical investigations show that hyperthermia in combination with radiotherapy is an effective means of treating cancer [1]–[4]. In addition, many of these results demonstrate that the level of hyperthermic cytotoxicity and the sensitization of the tumor tissue to radiotherapy rise exponentially with temperature [5], [6]. The result of treatment thus crucially depends on the capacity of the hyperthermia system to attain a controlled temperature hyperelevation of the entire target volume [7], [8]. Interstitial microwave antennas are especially suitable for inducing hyperthermia of deep-seated tumors (e.g. certain brain tumors), since a homogeneous distribution of electromagnetic energy in the target volume also entails the expectation of an almost homogeneous stable temperature hyperelevation in the target volume except when there are major temperature gradients in the vicinity of large vessels. A "thermal washout" by flow of blood, such as can be observed in the use of ferromagnetic seeds or radio frequency needles, occurs to a much lesser extent here [9]. Inter alia, the distribution of the electromagnetic field can be adapted to the respective target volume by the form and arrangement of the interstitial microwave antennas. The plastic catheters used in interstitial combination therapy (radiotherapy/hyperthermia) can be used to accommodate both, e.g. radioactive iodine seeds and microwave antennas.

Manuscript received July 16, 1990; revised December 19, 1990. This work was supported by the Deutsche Krebshilfe.

The authors are with the Department of Radiology and Pathophysiology, German Cancer Research Center, Heidelberg, Germany.

IEEE Log Number 9144270.

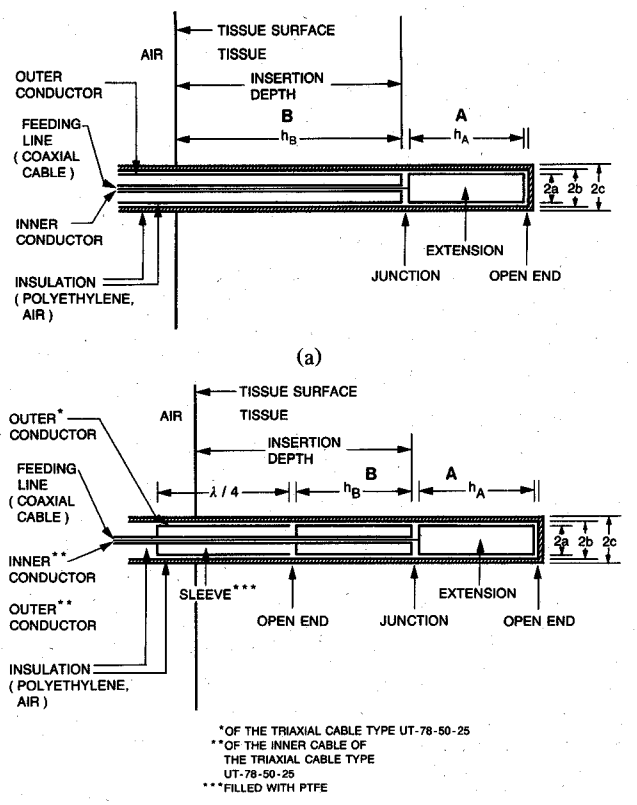

Fig. 1. (a) Conventional antenna (figure not to scale). (b) New dipole antenna with $\lambda/4$ sleeve and transformed open end (figure not to scale).

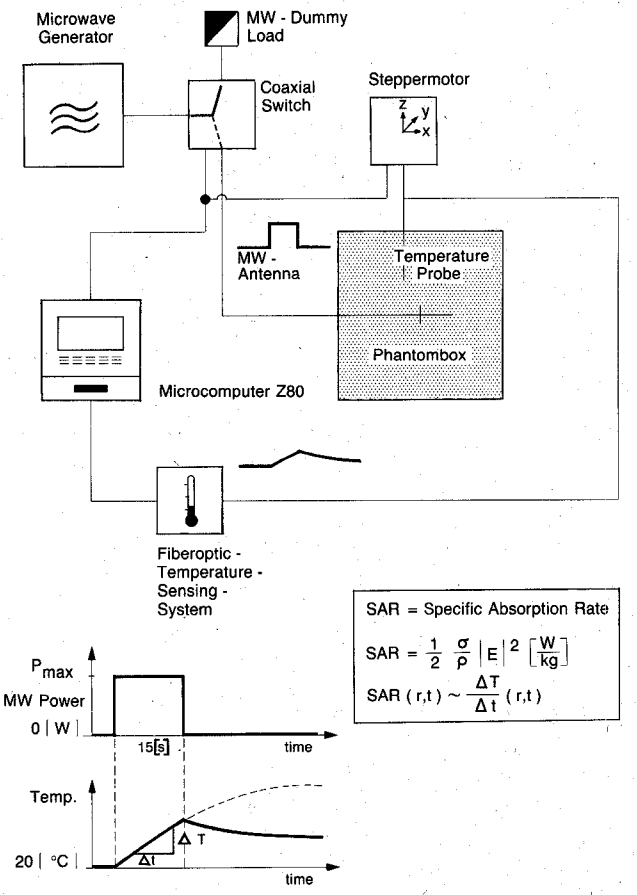

Fig. 2. Experimental setup for the SAR measurements.

The interstitial microwave antennas used at present basically consist of a coaxial cable at one end of which the inner conductor is connected to an extension e.g. with the diameter of the outer conductor (Fig. 1(a)). The coaxial cable and extension are encapsulated in an insulating sheath, for example PTFE. This applicator was first presented in 1978 by Taylor [10]. The disadvantage of this design derives from the fact that its power deposition pattern depends on the insertion depth [11]. Along the outer conductor of the cable there is a backward current in the direction of the generator which can lead to an uncontrolled heating of surrounding tissue. This effect could not be eliminated by using antennas with an enlarged collar on the extension and the outer conductor [12]. This paper describes a sleeve dipole antenna to reduce the back flow current seen on conventional antennas. The power deposition pattern is therefore less dependent on the insertion depth.

II. Methods and Materials

A. Antenna Design

According to King *et al.* [11] the input impedance of a coaxial transmission line equals

$$Z_{\text{in}} = 1/Y_{\text{in}} = -i \cdot Z_c \cdot \tan(k_l \cdot h + i\Theta_h) \qquad (1)$$

where Y_{in} is the admittance, Z_c the characteristic impedance, k_l the wavenumber, and h the length of the transmission line.

The terminal function

$$\Theta_h = \coth^{-1}(Z_h/Z_c)$$

equals zero at $Z_h = \infty$ (open end) and equals $-i \cdot \pi/2$ at $Z_h = 0$ (short-circuit end). By operating two coaxial transmission line sections (A and B) in series, the total impedance Z terminating the feeding line equals

$$Z = Z_{\text{in}A} + Z_{\text{in}B}.$$

The conventional applicator is made of a transmission line with a constant length h_A and an open end terminating impedance. Thus its input impedance can be defined by (1). The length of the second transmission line (B) varies according to insertion depth and does not have an open or short-circuited end terminating impedance. Therefore the total input impedance of the applicator is variable. The power consumptions of the two transmission line sections as well as the power distributions vary according to different input impedances. Power can flow back along the outer conductor of the feeding line in the direction of the generator, and, depending on the power distribution, this leads to a uncontrolled heating of the surrounding medium in region B. In contrast to these phenomena, the applicator described in this paper (Fig. 1(b)) consists of a coaxial transmission line B having a definite length, h_B, seeing an open end terminating impedance due to the $\lambda/4$ sleeve ($\pi/2$ transformer). Transmission line section A remains unchanged. Thus the input impedance of transmission line B defined by (1) is independent of the insertion depth into the dissipative medium. Hence power uptake and power distribution of the total applicator are defined. The total amount of the power fed into the antenna is transported through transmission line A and transmission line B into the surrounding dissipative medium. A backflow of power along the outer conductor of the feeding line to the generator

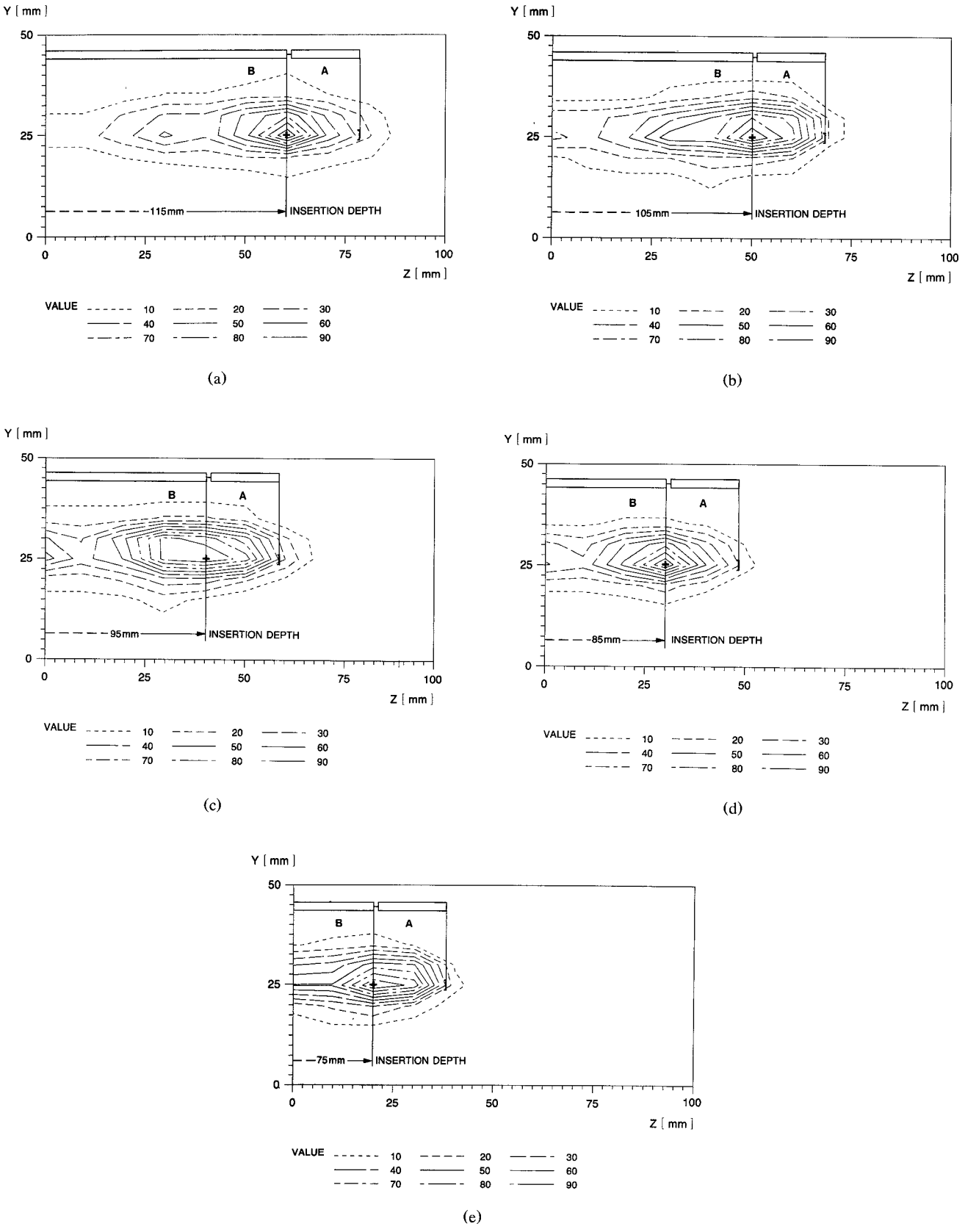

Fig. 3. Conventional antenna. (a) Insertion depth: 115 mm. (b) Insertion depth: 105 mm. (c) Insertion depth: 95 mm. (d) Insertion depth: 85 mm. (e) Insertion depth: 75 mm.

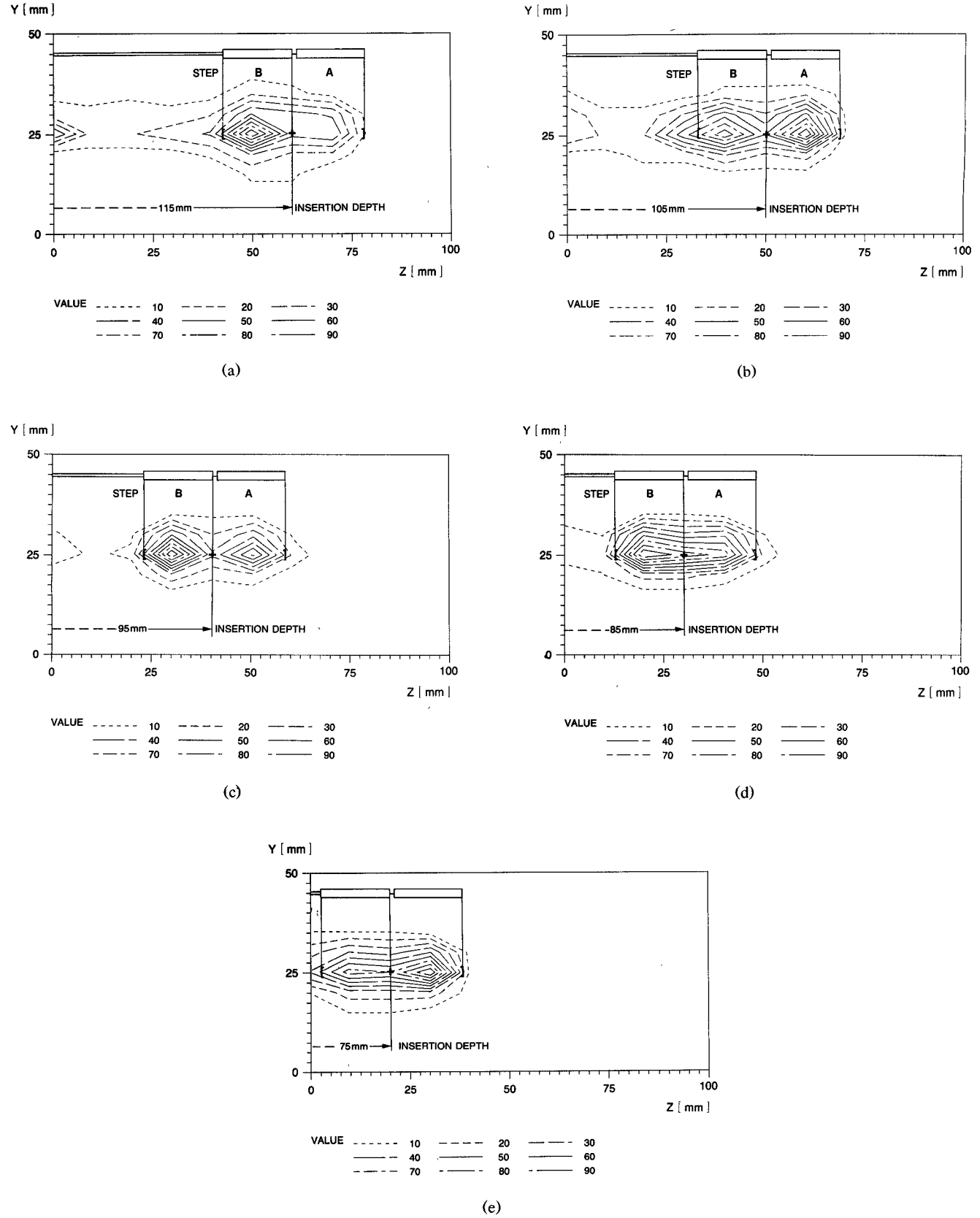

Fig. 4. Modified conventional antenna. (a) Insertion depth: 115 mm. (b) Insertion depth: 105 mm. (c) Insertion depth: 95 mm. (d) Insertion depth: 85 mm. (e) Insertion depth: 75 mm.

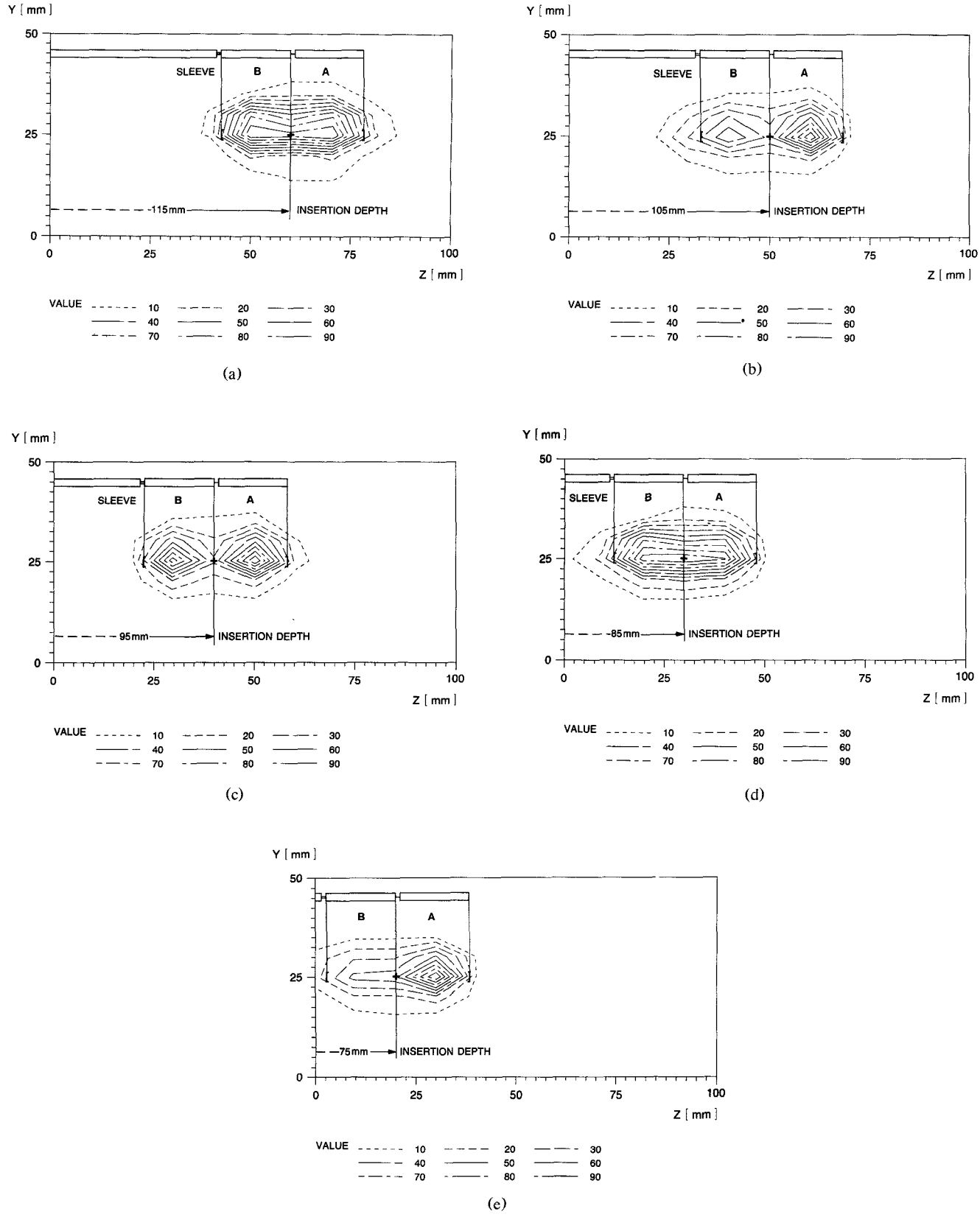

Fig. 5. New dipole antenna. (a) Insertion depth: 115 mm. (b) Insertion depth: 105 mm. (c) Insertion depth: 95 mm. (d) Insertion depth: 85 mm (e) Insertion depth: 75 mm.

and, consequently, a potential heating up of normal tissue are prevented.

B. Experimental Setup

SAR measurements at 915 MHz reveal the advantages of the new antenna. As a dissipative medium, a phantom consisting of 62.61% H_2O, 29.8% polyethylene powder (20-mesh, low-density, BASF AG, Ludwigshafen, FRG), 7.01% TX 150 gelling agent (Oil Center Research, Lafayette, U.S.), and 0.58% NaCl was used. The complex permittivity of the phantom corresponds to that of brain tissue at 915 MHz [13]. Fig. 2 shows the experimental setup for the SAR measurements. Controlled by a Z80 microcomputer and guided by a stepper motor, a fiber-optic temperature probe (Luxtron 1000B) is moved perpendicular to the antenna's axis in PTFE catheters (1.0 mm inner diameter, 1.5 mm outer diameter) at a distance of 5 mm from the antenna's axis in steps of 5 mm each. The distance between the axes of any two catheters is 10 mm. Therefore the resolution of the SAR distribution along the antenna's axis is just half of the resolution in the perpendicular direction. At each position the temperature is measured during a 15 s, 10 W microwave pulse, and the temperature gradient is calculated by the linear regression method. Ten minutes after switching off the microwave power the measurement is restarted at the next position in the phantom material. A matrix of 11×11 data is set up. The complete SAR distribution is then calculated using the parabolic interpolation method. The iso-SAR contours are graded at 10% intervals and the maximum value is set to a value of 100%.

For a direct comparison, three antennas were constructed with the triaxial cable type UT 78-50-25 from UTI (Micro-Coax Components, Collegeville, U.S.). The radii of the antennas (see also parts (a) and (b) of Fig. 1) are

- a: 0.99 mm (outer radius of the metallic conductor of the antennas);
- b: 1.015 mm (inner radius of the insulating polyethylene sheaths);
- c: 1.11 mm (outer radius of the insulating polyethylene sheaths).

Other data are as follows:

- insulation: polyethylene and air (LD-PE 3032D, $\epsilon' = 2.3$);
- length of the $\lambda/4$ antennas: 16.8 mm (resonant length);
- characteristic impedance Z_c: $36.7 - 12.5i\ \Omega$;
- input impedance Z_{in}: $13.8 + 4.7i\ \Omega$ at $\lambda/4$;
- α_l/β_l: 0.252, where α_l and β_l are the imaginary and real parts of the complex propagation constant $k_l = \beta_l + i\alpha_l$.

The resonant length of the antennas, the characteristic impedance Z_c, the input impedance Z_{in}, and the complex propagation constant k_l were calculated according to King *et al.* [11]. The resonant lengths of the antennas were always held constant; this means that in the case of the conventional antenna only the extension of the antenna had this resonant length. In the cases of the modified conventional antenna and the new antenna, the extension (section A with length h_A) and section B with length h_B (on the feeding line) had this resonant length. The polyethylene sheaths were custom-made thin-walled plastic tubes.

III. Results and Discussion

Parts (a)–(e) of Fig. 3 show the conventional antenna at insertion depths of 115, 105, 95, 85, and 75 mm. These are the distances along the feeding line of the antenna between the surface of the phantom and the junction. The feeding line runs from the left at $Y = 25$ mm parallel to the Z axis and parallel at a 5 mm distance to the measured SAR plane. Note that a large amount of power runs back on the outer conductor of the feeding line toward the generator.

Parts (a)–(e) of Fig. 4 show a modified conventional antenna in phantom positions corresponding to those of the antenna in Fig. 3 but with a reduction of the outer diameter of the feeding line. Symmetrical to the junction there now emerges an impedance step for the backward-running current. At the impedance step the radius has been reduced from 0.99 mm to 0.43 mm. Note that the backward-running power creates a hot area on the lower half of the antenna and another one at the left of the diagram at $Z = 0$ mm and $Y = 25$ mm. The left bracket represents the impedance step on the outer conductor of the feeding line, which means from this location along the feeding line toward the generator the radius of the feeding line of the antenna has been reduced from 0.99 mm to 0.43 mm. The right bracket represents the tip of the antenna.

Parts (a)–(e) of Fig. 5 show the SAR pattern of the newly developed dipole antenna with a $\pi/2$ transformer ($\lambda/4$ sleeve) on the feeding line which concentrates the power on the dipole antenna irrespective of the insertion depth. The variations of the SAR contours of the new antenna with different insertion depths may be attributed, among other factors, to an eccentric position of the antenna in the polyethylene sheath and to inhomogeneities of the phantom material with regard to the complex permittivity. It was observed by a directional coupler between the microwave generator and the applicator during the SAR experiments that, in contrast to the conventional applicator, the new applicator showed a considerable independence between insertion depth and reflected power. The impedance of the newly developed applicator remained constant regardless of the insertion depth into the phantom. (*Condition*: Section A and section B of the applicator must be completely surrounded by the dissipative medium.)

IV. Conclusion

The radiation characteristics of conventional interstitial microwave hyperthermia antennas depend to a considerable extent on the insertion depth of the applicator into the tissue. Therefore the use of these antennas involves risk since an overheating of normal tissue caused by uncontrollable microwave energy deposition along the feeding line cannot be ruled out. As shown by the SAR measurements of the new antenna, this disadvantage is avoided by transforming an open end at the generator end of the dipole. The target volume can be precisely irradiated. There is good reason to believe that the new antenna will prove to be ideal for interstitial hyperthermia. Moreover, it can be employed in all cases that allow the use of interstitial or intracavitary high-frequency applicators.

References

[1] G. Arcangeli, M. Benassi, A. Cividalli, G. A. Lovisolo, and F. Mauro, "Radiotherapy and hyperthermia: Analysis of clinical results and identification of prognostic variables," *Cancer*, vol. 60, pp. 950–956, 1987.

[2] M. W. Dewhirst and D. A. Sim, "Estimation of therapeutic gain in clinical trials involving hyperthermia and radiotherapy," *Int. J. Hypertherm.*, vol. 2, no. 2, pp. 165–178, 1986.

[3] J. Overgaard, "Hyperthermia as an adjuvant to radiotherapy," *Strahlentherapie Onkol.*, vol. 163, pp. 453–457, 1987.

[4] C. A. Perez, B. Emami, G. H. Nussbaum, and S. A. Sapareto, "Hyperthermia," in *Principles and Practice of Radiaton Oncology*. Philadelphia, PA: J. B. Lippincott, 1987, pp. 317–352.
[5] W. C. Dewey, *et al.*, "Cell biology of hyperthermia and radiation," in *Radiation Biology in Cancer Research*, R. Meyn and R. Withers, Eds. New York: Raven Press, 1980, pp. 589–621.
[6] M. W. Dewhirst, D. A. Sim, S. A. Sapareto, and W. G. Connor, "The importance of minimum tumor temperature in determining early and long-term responses of spontaneous pet animal tumors to heat and radiation," *Cancer Res.*, vol. 44, pp. 43–50, 1985.
[7] T. C. Cetas, and R. B. Roemer, "Thermal dosimetry: Four aspects," *Front Radiat. Oncol.*, vol. 18, pp. 75–82, 1984.
[8] M. D. Sapozink, F. A. Gibbs, Jr., and T. S. Sandhu, "Practical thermal dosimetry," *Int. J. Radiat. Oncol. Biol. Phys.*, vol. 11, pp. 555–560, 1985.
[9] J. A. Mechling and J. W. Strohbehn, "A theoretical comparison of the temperature distributions produced by three interstitial hyperthermia systems," *Int. J. Radiat. Oncol. Biol. Phys.*, vol. 12, pp. 2137–2149, 1986.
[10] L. S. Taylor, "Devices for microwave hyperthermia," in *Cancer Therapy by Hyperthermia and Radiation*, C. Streffer, Ed. Baltimore: Urban & Schwarzenberg, 1978, pp. 115–117.
[11] R. W. P. King, L. C. Shen, and T. T. Wu, "Embedded insulated antennas for communication and heating," *Electromagnetics*, vol. 1, pp. 115–117, 1981.
[12] A. M. Tumeh and M. F. Iskander, "Performance comparison of available interstitial antennas for microwave hyperthermia," *IEEE Trans. Microwave Theory Tech.*, vol. 37, pp. 1126–1133, 1989.
[13] C. K. Chou, G. W. Chen, A. W. Guy, and K. H. Luk, "Formulas for preparing phantom muscle tissue at various radiofrequencies," *Bioelectromagnetics*, vol. 5, pp. 435–441, 1984.

DC Conduction and Low-Frequency Noise Characteristics of GaAlAs/GaAs Single Heterojunction Bipolar Transistors at Room Temperature and Low Temperatures

V. K. Raman, C. R. Viswanathan, and Michael E. Kim

Abstract—**The dc conduction and low-frequency noise characteristics of GaAlAs/GaAs single heterojunction bipolar transistors (HBT's) have been investigated at room temperature and at temperatures down to 5 K. The I_c dependence of the current gain has been investigated at various temperatures. The low-frequency noise characteristics exhibit both $1/f$ and generation–recombination (g–r) components. The noise characteristics are sensitive to changes in base current and insensitive to changes in V_{ce}, thus suggesting that the noise source is located in the vicinity of the emitter–base heterojunction. The noise spectrum follows a simple model based on minority carrier trapping effects at the heterointerface.**

I. Introduction

The GaAlAs/GaAs heterojunction bipolar transistor is gaining considerable interest as an excellent low $1/f$ noise device for analog/microwave, digital, and A/D conversion applications [1], [2]. Since the carriers are injected from a wider band gap GaAlAs emitter to a narrow band gap GaAs base, one can engineer the doping in the emitter region such that a lightly doped region occurs near the emitter–base junction while the rest of the emitter is heavily doped for contact purposes. The base region too can be heavily doped without affecting the injection efficiency. This results in a considerable reduction in emitter–base junction capacitance and base series resistance and hence a remarkable improvement in speed. With a heavy base doping, phenomena such as emitter crowding, base width modulation, and punch-through effects are also minimized, resulting in better performance of the device. Since there are problems associated with realizing collector–base heterojunctions with good electrical characteristics, the single HBT's are emerging as devices much superior to DHBT's. Though the high-frequency noise has been investigated in detail by several authors, the low-frequency noise behavior of these technologically important devices has been studied much less. The low-frequency noise is a key parameter of interest from the point of view of reliability, phase noise, and an understanding of the effects of trapping on device performance [3], [4].

No unified theory exists for low-frequency $(1/f)$ noise behavior, even for conventional homojunction bipolar transistors (BJT's), although experimental evidence suggests that defects and surface states at the emitter–base junction are responsible for the noise [5]. A mobility fluctuation model based on Hooge's hypothesis [6] has also been proposed [7] and contradicted by several results [8]. A simple method of implementing the natural feedback action of actively biased devices has been utilized to locate the low-frequency noise generator in bipolar transistors [9], [10]. The results published so far indicate that there is no clear understanding of the exact physical origin of the noise for the conventional BJT's. The situation is worse for the complex HBT's. Blasquez *et al.* [11] have studied the current noise in GaAlAs/GaAs HBT's and reported that the devices displayed a small $1/f$ noise at low frequencies and a fairly high level of recombination noise at intermediate and high frequencies. Low-frequency noise measured in high-current-gain GaAs/GaAlAs DHBT's has been shown [3] to originate from the base and is found to be interface $1/f$ and generation–recombination (g–r) noise. All these measurements have been done at room temperature. There are certain unique advantages in operating these devices at lower temperatures, such as mobility enhancement and hence higher speed. Thus it is extremely important to understand the conduction properties and the low-frequency noise behavior at lower temperatures for cryoelectronic applications. In this paper we report the dc conduction and low-frequency noise characteristics of GaAlAs/GaAs SHBT's at room temperature and at temperatures down to 5 K. The devices exhibit stable characteristics at low temperatures and the offset voltage is slightly reduced at lower temperatures. The low-frequency noise spectra exhibit both $1/f$ and g–r components and the presence of g–r components is possibly due to distributed traps at the heterointerface. The noise spectra follow a model based on minority carrier trapping effects at the heterointerface.

II. Experimental

The cross section of a typical HBT structure, illustrated schematically in Fig. 1, is part of an integrated circuit process [2]. The main feature of the structure is the self-aligned base

Manuscript received August 20, 1990; revised January 17, 1991. This work was supported by TRW and by the state of California through the 1988–89 MICRO Program.

V. K. Raman and C. R. Viswanathan are with the Electrical Engineering Department, University of California, Los Angeles, CA 90024.
M. E. Kim is with the TRW Electronics and Technology Division, One Space Park, Redondo Beach, CA 90278.

IEEE Log Number 9144267.